Geochemistry Geophysics Geosystems G3
AN ELECTRONIC JOURNAL OF THE EARTH SCIENCES
Published by AGU and the Geochemical Society

Article
Volume 9, Number 6
24 June 2008
Q06011, doi:10.1029/2007GC001896
ISSN: 1525-2027

Dynamics of core formation and equilibration by negative diapirism

H. Samuel
Bayerisches Geoinstitut, Universität Bayreuth, D-95440 Bayreuth, Germany (henri.samuel@uni-bayreuth.de)

Institut für Geophysik, ETH Zürich, CH-8093 Zürich, Switzerland

P. J. Tackley
Institut für Geophysik, ETH Zürich, CH-8093 Zürich, Switzerland (ptackley@ethz.ch)

[1] We investigate dynamically the timing and metal-silicate equilibration processes during core formation by negative diapirism. Using numerical modeling in 3-D axisymmetric geometry, we follow the sinking of iron-rich diapirs through a viscous silicate mantle. We carried out a parameter study in which shear heating as well as several viscous rheologies are considered and systematically varied. General scaling laws are derived for the diapir sinking velocity as well as for the silicate melt generation and distribution around the diapir. Using these scaling laws, we show that metal diapirs of a radius $\sim$1–100 m, sinking through a partially molten silicate mantle can chemically equilibrate within the timescales suggested by geochemical constraints. Therefore negative diapirism can contribute significantly to metal-silicate equilibration processes during core formation.

Components: 7751 words, 9 figures, 2 tables.

Keywords: core formation; viscous heating; Stokes velocity; Fe-Si equilibration.

Index Terms: 8125 Tectonophysics: Evolution of the Earth (0325); 8115 Tectonophysics: Core processes (1213, 1507); 8124 Tectonophysics: Earth's interior: composition and state (1212, 7207, 7208, 8105).

Received 15 November 2007; **Revised** 17 March 2008; **Accepted** 8 April 2008; **Published** 24 June 2008.

Samuel, H., and P. J. Tackley (2008), Dynamics of core formation and equilibration by negative diapirism, *Geochem. Geophys. Geosyst.*, *9*, Q06011, doi:10.1029/2007GC001896.

1. Introduction

[2] Several terrestrial planets and satellites possess a metallic core surrounded by a silicate mantle. Core formation by metal-silicate separation is thought to have happened during or right after the first stages of planetary accretion, 4.5 billion years ago [e.g., *Kleine et al.*, 2004a, 2004b]. Core formation is therefore the first major differentiation event that has determined the initial thermochemical state of several terrestrial planets.

[3] The processes that led to metal-silicate separation in terrestrial planets are still debated and several possible scenarios have been proposed [*Stevenson*, 1981]. However, constraints on core formation are provided by geochemical and mineral physics considerations. The most obvious constraint is the need for temperatures above the

silicate melting point in order to separate efficiently metal from silicates. This requirement is supported by accretional models, which show that once a growing planet reaches a radius of ~2000 km, the energy provided by incoming impacts leads to temperatures above the silicate solidus [*Coradini et al.*, 1983; *Sasaki and Nakazawa*, 1986; *Senshu et al.*, 2002]. Furthermore, a giant impact stage, thought to have occurred on Earth, would have provided enough energy to entirely melt and partially vaporize the Earth [e.g., *Canup*, 2004]. Timing constraints on core formation are provided by geochemical considerations with W/Hf systematics and suggest that the timescale for core formation is on the order of 10–100 Ma for the Earth or Mars [*Kleine et al.*, 2004a, 2004b]. Additional constraints are provided by the overabundance of moderately siderophile elements (e.g., Ni, Co) in the Earth's mantle, which suggests that complete or partial equilibration has occurred between the metal and the silicates during core formation [*Ringwood*, 1966; *Karato and Murthy*, 1997; *Rubie et al.*, 2003, 2007; *Halliday*, 2004; *Wood et al.*, 2006].

[4] Melting at local or global scales is the starting point for metal-silicate separation and core formation. This has led to several possible core formation scenarios as proposed by *Stevenson* [1981] (see also *Rubie et al.* [2007] for a recent review). Several authors have focused on the ability of a particular scenario to meet the timing and/or the equilibration constraints provided by geochemistry and mineral physics. This type of exercise is fundamental in determining the initial conditions from which many terrestrial planets have evolved.

[5] For instance, previous studies (*Karato and Murthy* [1997], *Rubie et al.* [2003], and more recently *Hoïnk et al.* [2006]) have focused on the kinetics of core formation via metal "rain fall". In this scenario, cm-sized metal droplets sink within a vigorously convecting global silicate magma ocean. These studies have shown that metal-silicate equilibration is possible in such a context during the sinking of the metal droplets. However, once the denser metal droplets accumulate at the bottom of the magma ocean, forming a global iron layer, equilibration processes are too slow to occur efficiently. Indeed, the short timescale for the solidification of a magma ocean (~1000 years [*Solomatov*, 2000]) quickly drives temperatures below the silicate solidus. Consequently, equilibration processes become controlled by the very low chemical diffusivities of solid silicate, thus preventing metal-silicate equilibration within a reasonable time period [*Rubie et al.*, 2003].

[6] As suggested by various studies [e.g., *Stevenson*, 1981; *Sasaki and Nakazawa*, 1986; *Senshu et al.*, 2002; *Rubie et al.*, 2003; *Hoïnk et al.*, 2006] the accumulation of iron at rheological boundaries leads to a gravitationally unstable configuration where a global iron layer surrounds a colder, less dense, protocore. The timescale of core formation by Rayleigh-Taylor destabilization of such a dense iron layer has been studied by *Honda et al.* [1993] using numerical modeling in cylindrical geometry without temperature or stress-dependent viscosity. Their results show that core formation with this mechanism can be achieved in a reasonable time frame if the protocore viscosity is less than 10^{26} Pa s. However, the consequences for metal-silicate equilibration were not investigated and viscous heating was not taken into account.

[7] An alternative core formation scenario is the sinking of large iron diapirs that originate at the surface of a growing planet where magma ponds are formed [*Stevenson*, 1981; *Senshu et al.*, 2002] or at the bottom of a magma ocean [*Rubie et al.*, 2003]. This scenario was investigated analytically by *Karato and Murthy* [1997]. The authors concluded that core formation by negative diapirism could not explain the observed overabundance of siderophile elements in the Earth's mantle because the large size of the iron diapir would not allow metal and silicate equilibration. However, these calculations were conducted only for Newtonian rheologies and did not take into account the generation of heat and melting via viscous dissipation. This mechanism is likely to generate a temperature increase in the vicinity of the diapir and therefore to favor metal-silicate equilibration by increasing significantly the chemical diffusivity of silicate material.

[8] Therefore, in this paper we examine dynamically the timing and metal-silicate equilibration processes during core formation by negative diapirism. We use high-resolution numerical modeling to follow the sinking of iron-rich diapirs through a viscous silicate mantle in a 3-D axisymmetric geometry. We conducted a parameter study in which shear heating as well as several viscous rheologies are considered and systematically varied. General scaling laws are derived for the diapir sinking velocity as well as for the heat/melt distribution. We subsequently use these scaling laws to

investigate the ability of negative diapirism to form a metallic core in terrestrial planets within the timing and metal-silicate equilibration constraints provided by geochemistry and mineral physics.

2. Dynamics of Negative Diapirism

[9] We perform a series of numerical experiments in order to study the dynamics of a metal diapir sinking through a solid or partially molten silicate mantle.

2.1. Numerical Setup

[10] The four governing equations for the system, under the extended Boussinesq approximation and in the limit of infinite Prandtl number, are the conservation of mass:

$$\nabla \cdot \mathbf{U} = 0, \tag{1}$$

the conservation of momentum:

$$\nabla p - \nabla \cdot \left(\eta \dot{\varepsilon}_{ij}\right) + Ra(T - BC)\vec{e}_r = 0, \tag{2}$$

the conservation of energy:

$$\frac{DT}{Dt} = \nabla^2 T + \frac{Di}{Ra}\phi_v - DiTU_r. \tag{3}$$

and the conservation of a compositional field C used to model the presence of iron (C = 1) or silicate material (C = 0)

$$\frac{DC}{Dt} = 0. \tag{4}$$

[11] These equations are expressed in terms of dimensionless variables: $\mathbf{U}$ is the velocity vector, p is the dynamic pressure, η is the viscosity, T is the temperature, t is the time, U_r is the radial component of the velocity, and $\vec{e}_r$ is a unit vector along the radial axis and pointing outward. $\phi_v = \sigma_{ij} : \dot{\varepsilon}_{ij}$ is the dissipation function where $\sigma_{i\ j}$ is the deviatoric stress tensor and $\dot{\varepsilon}_{ij}$ is the strain rate tensor.

[12] The characteristic scales used to normalize the four governing equations are the total silicate-mantle thickness H, the silicate density ρ_0, a characteristic temperature difference ΔT, and the silicate-mantle viscosity η_0. The thermal diffusion timescale, H^2/κ_T, is used where $\kappa_T = 10^{-6}$ m^2 s^{-1} is the thermal diffusivity.

[13] Three nondimensional numbers appear from the normalization of the conservation equations and define the parameter space of the system. The first is the Rayleigh number, $Ra = (\rho_0 \alpha \Delta T g H^3)/(\eta_0 \kappa_T)$, where g is the gravitational acceleration and α is the thermal expansion coefficient. The second is the buoyancy number, $B = \Delta\rho_c/(\rho_0 \alpha \Delta T)$, where $\Delta\rho_c$ is the compositional density contrast between the metal diapir and the silicate material. The third is the dissipation number, $Di = \alpha g H/C_p$, where C_p is the specific heat at constant pressure.

[14] The four conservation equations are solved numerically using the finite volume code STAGYY in spherical axisymmetric geometry (P. J. Tackley, Modelling compressible mantle convection with large viscosity contrasts in a three-dimensional spherical shell using the yin-yang grid, submitted to *Physics of the Earth and Planetary Interiors*, 2008). Equation (4) is solved using a tracer ratio technique with a mass error [*Tackley and King*, 2003] lower than 1%. In order to avoid significant numerical diffusion, the advective part of equation (3) is also solved using a Lagrangian approach as described by *Gerya and Yuen* [2003]. The computational domain is composed of 512 to 1024 regular cells in each direction, ranging from 4.0 to 5.0 and 0.0 to 0.15 in the radial and angular directions, respectively. In order to reduce the wall effects on the flow [*Chang*, 1961], the distance between the diapir and the side wall opposite to the axis of symmetry is at least ten times the initial radius of the spherical diapir (less than 0.04 in our experiments). The temperature is set constant at the outer surface while the temperature flux is set to 0 on all the other surfaces. Free slip velocity boundary conditions are imposed on all boundaries. Note that the following results correspond to cases where the sinking diapir is far from any boundary (apart from the axis of symmetry), therefore the nature of the boundary conditions we impose plays a minor role.

[15] We consider several rheologies where the viscosity can be dependent on composition, temperature and/or melt fraction and stress:

$$\eta(C, T, melt, \sigma) = \frac{\eta_0 e^{[-\ln(\gamma_T)T_p]}}{1 + C(\gamma_c - 1)}\left[1 + \left(\frac{\sigma}{\sigma_T}\right)^{n-1}\right]^{-1} \tag{5}$$

where T_p is the potential excess temperature. The iron diapir is assumed to be much less viscous than the surrounding silicate mantle because of the lower solidus for iron, therefore the viscosity ratio

between the silicate mantle and the iron diapir is $\gamma_c = 10^3$. A higher value for γ_c would be more realistic but should not affect our results [*Hadamard*, 1911; *Rybczynski*, 1911]. n is the power law index, σ_T is the dimensionless transition stress at which material flows equally via dislocation and diffusion creep. Viscosity dependence on temperature and melt fraction is treated in a similar way with the parameter γ_T. In some cases we use a temperature threshold T_r above which viscosity is abruptly decreased by a factor $\gamma_r = 10^5$. This is done in order to mimic the effect of the rheological transition which occurs in silicates when the melt volume fraction exceeds a critical value of about 60–70% [*Lejeune and Richet*, 1995; *Scott and Kohlstedt*, 2006]. For numerical stability we impose a viscosity cutoff $\eta = MAX(\eta, \eta_0 \times 10^{-5})$.

[16] Density, ρ, varies according to the linear equation of state:

$$\rho = \rho_0\left[1 - \alpha T_p\right] + C\Delta\rho_c. \tag{6}$$

[17] This model setup shares some similarities with previous numerical and laboratory experiments that were studying the motion of rigid or free-slip diapirs, in temperature-dependent medium [e.g., *Morris*, 1982; *Ribe*, 1983; *Daly and Raefsky*, 1985; *Mahon et al.*, 1988; *Ziethe and Spohn*, 2007; *Ricard et al.*, 2008; *Golabek et al.*, 2008, and references therein], with, however, several important differences. In our study both viscous heating and nonlinear rheologies are considered. Additionally, in contrast to previous work (with the exception of *Ricard et al.* [2008] and *Golabek et al.* [2008] carried in 2-D cartesian geometry) melt-dependent viscosity was considered and the diapir in our experiments is deformable.

2.2. Results

[18] As previously mentioned, the dynamics of the system is governed by *Ra*, *B*, and *Di*. However, one can reduce this parameter space by noticing that the compositional density contrast $\Delta\rho_c \sim 4500$ kg/m^3 is much greater than the thermal density contrast ($\sim$1 to at most few hundreds of kg/m^3). Therefore, although the thermal density contrast are taken into account in our models, $B \gg 1$ one can reasonably neglect the influence of *Ra* on the flow (compared to that of *RaB*) in our numerical experiments. We checked that this assumption was reasonable by varying separately *Ra* and *RaB*. As expected, we found that the results (velocity and thermal evolution) mainly depend on *RaB* only rather than on both *Ra* and *RaB*.

[19] For similar reasons, viscous heating (second term on the right hand side of equation (3)) largely dominates over adiabatic heating (third term on the right hand side of equation (3)). As a consequence, the parameter space is reduced to two dimensionless parameters: the compositional Rayleigh number,

$$R_b = RaB = \frac{\Delta\rho_c g H^3}{\eta_0 \kappa_T}. \tag{7}$$

and a second parameter which expresses the efficiency of viscous heating

$$H_v = \frac{Di}{Ra} = \frac{\eta_0 \kappa_T}{\rho_0 \Delta T C_p H^2}. \tag{8}$$

[20] We therefore systematically investigate the influence of R_b and H_v for various viscous rheologies. In the following sections we consider separately the behavior for Newtonian and power law cases, as well as the influence of temperature-/melt-dependent viscosity. As a common initial condition for all our numerical experiments, we start with a spherical metal diapir of radius r_d located along the axis of symmetry, close to the outer surface of our model domain (at a distance 4.9 on the radial axis) with a positive homogeneous dimensionless potential temperature excess. Inside the diapir the dimensionless viscosity is γ_c^{-1}, while outside of the diapir, the viscosity is 1.

2.2.1. Typical Evolution of a Newtonian Case With Constant Viscosity

[21] When viscosity does not depend on temperature or melt fraction, the parameter H_v does not affect the flow nor the diapir sinking velocity V_s. This case is similar to several numerical experiments carried by *Daly and Raefsky* [1985] with the exception that in our model the sphere is deformable. We find, as expected, that the diapir sinking velocity quickly reaches a constant value close to the Stokes velocity, V_0, for a frictionless sphere whose viscosity is small compared to the surrounding viscosity η_0 [*Hadamard*, 1911; *Rybczynski*, 1911]:

$$V_0 = \frac{1}{3}\frac{\Delta\rho_c g r_d^2}{\eta_0}. \tag{9}$$

[22] This is illustrated by the blue squares in Figure 1 which correspond to a Newtonian case with $H_v = 7.5 \times 10^{-8}$, $R_b = 3 \times 10^8$, $r_d = 0.03$ and $\gamma_T = 1$. The small difference between the numerical experiments and the theoretical value of V_0 (around

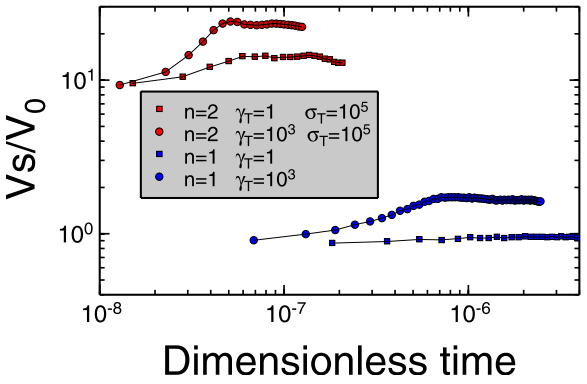

Figure 1. Results from the numerical experiments: dimensionless time evolution of diapir sinking velocities for four cases. Red symbols correspond to power law rheologies with n = 2 and $\sigma_T = 10^5$ (dimensionless). Blue symbols correspond to Newtonian cases. Squares indicate no temperature-dependent viscosity ($\gamma_T = 1$) while circles represent temperature-dependent viscosity with $\gamma T = 1000$.

5%) can be explained by the side wall effect [*Chang*, 1961]. This influence was confirmed by the various experiments carried out for different values of R_b with $\gamma_T = 1$.

[23] Additional features of this case are illustrated by Figures 2a and 2b which display the dimensionless viscous dissipation ϕ_v and the excess potential temperature T_p, respectively. At each stage ϕ_v inside the diapir is negligible because of the much lower viscosity within the iron-rich diapir. Outside the diapir, viscous dissipation is maximum at the diapir's poles and decreases rapidly toward the diapir's "equator" or with increasing distance r_c from the center of the diapir (Figure 2a). The distribution of ϕ_v outside the diapir can be predicted by using the analytical expression of the flow outside a sinking frictionless sphere [*Hadamard*, 1911; *Rybczynski*, 1911]. This implies that $\phi_v \sim \eta(\|\vec{r_c}\|)^{-2} V_s r_d \cos\theta)^2$, where $\vec{r_c}$ is a vector originating at the diapir's center and $\theta = (\vec{e_r}, \vec{r_c})$. As a consequence, the maximum temperature increase is at the diapir's poles as well as along the tail left behind the sinking diapir (Figure 2b) in good agreement with *Daly and Raefsky* [1985].

[24] In the absence of viscous heating ($H_v = 0$) the diapir's potential excess temperature inevitably converges toward 0 with time because of thermal diffusion. On the contrary, when $H_v > 0$ we consistently find a linear increase in the mean global potential temperature with increasing sinking distance of the diapir, regardless of any other parameters or rheologies. This linear relationship is the direct consequence of the conversion of the diapir's potential energy into thermal energy via viscous heating. A fraction of this thermal energy is transported from the silicate mantle to the diapir by thermal diffusion, leading to an increase in the diapir's temperature with time, as shown in Figure 2b.

[25] The increase of temperature due to viscous dissipation can range from few Kelvins to few thousands of Kelvins for a planet such as the Earth (i.e., with $H = 3000$ km, $\eta_0 = 10^{21}$ Pa s, $\Delta T = 1000$ K, $\rho_0 = 3500$ kg m^{-3}), depending on the size r_d of the iron diapir.

2.2.2. Influence of Temperature-/Melt-Dependent Viscosity

[26] Additional complexities occur when viscosity is temperature- or melt-dependent (i.e., $\gamma_T > 1$). Figure 3 displays three snapshots in a typical evolution of a system with a Newtonian rheology ($r_d = 0.03$, $H_v = 7.5 \times 10^{-8}$, $R_b = 3 \times 10^8$ and $\gamma_T = 10^3$). Similar to the constant viscosity case ($\gamma_T = 1$), ϕ_v inside the diapir is negligible because of the much lower viscosity within the iron-rich diapir (Figures 3a–3c). In addition, ϕ_v at the earliest stage (Figure 3a) compares well with the geometry and the magnitude found for the constant viscosity case (Figure 2a).

[27] However, as the diapir sinks, the higher-temperature tail left behind induces a lower-viscosity region (Figures 3e–3f and 3h–3i). This low-viscosity tail breaks the symmetry between

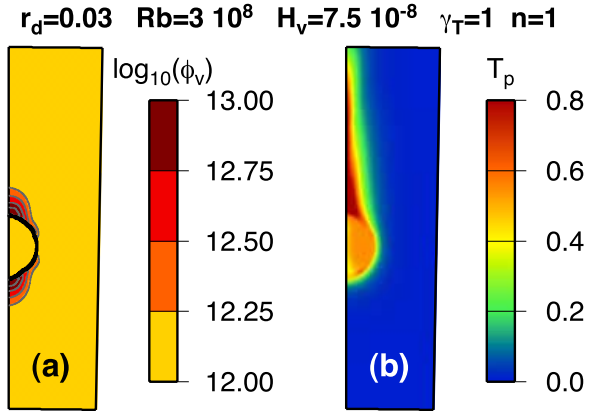

Figure 2. Results of the numerical experiment (close up view) for a Newtonian rheology, with $H_v = 7.5 \times 10^{-8}$, $R_b = 3 \times 10^8$, $r_d = 0.03$ and $\gamma_T = 1$. (a) Dimensionless viscous dissipation and (b) potential excess temperature for a dimensionless elapsed time t = 2.7×10^{-6}.

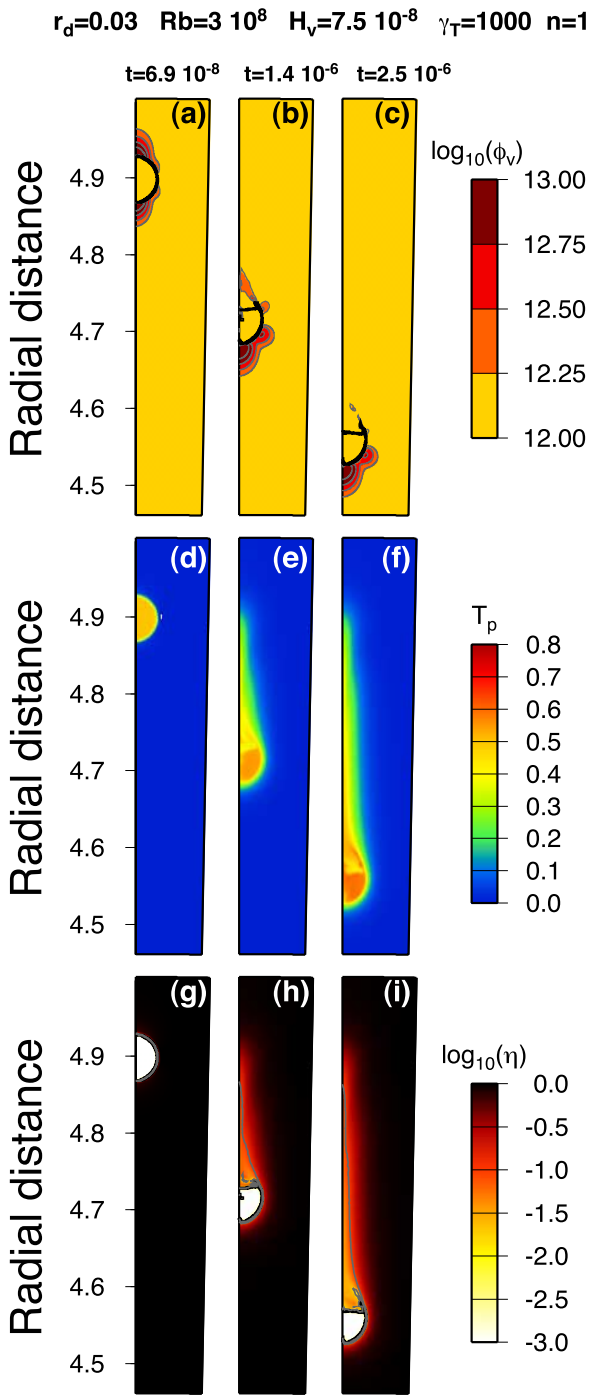

Figure 3. Results of the numerical experiment (close up view) for a Newtonian rheology, with $H_v = 7.5 \times 10^{-8}$, $R_b = 3 \times 10^8$, $r_d = 0.03$, and $\gamma_T = 1000$. (a–c) Dimensionless viscous dissipation, (d–f) potential excess temperature, and (g–i) viscosity for three different dimensionless elapsed times ($t = 6.9 \times 10^{-8}$, $t = 1.4 \times 10^{-6}$, and $t = 2.5 \times 10^{-6}$).

the upper and lower hemispheres of the sinking diapir and modifies the stress field, leading to a change of the diapir's shape from initially spherical to a hemispherical cup. During this transition, ϕ_v in the diapir's upper hemispherical region decreases significantly, while in the diapir's lower hemisphere region ϕ_v remains fairly constant (Figures 3a, 3d, and 3g).

[28] To quantify the effect of temperature-/melt-dependent viscosity on the diapir's sinking velocity we performed runs where the parameter γ_T in equation (5) was systematically varied. The results are shown in Figure 4 and indicate that the influence of γ_T on V_s can be described by a power law relationship:

$$\frac{V_s}{V_0} = f(\gamma_T) = \gamma_T^{0.06}. \tag{10}$$

[29] This relatively weak influence of γ_T on V_s is due to the very localized viscous heating and to the domination of heat advection over heat diffusion in our experiments (i.e., relatively high Péclet number). Therefore the far field pressure drag is not significantly affected by the value of γ_T. This means that localized viscosity variation due to temperature or to the presence of silicate melt is not likely to affect the diapir sinking velocity by more than one order of magnitude. This is in good agreement with previous numerical experiments by *Daly and Raefsky* [1985].

2.2.3. Effect of Non-Newtonian Rheology

[30] As seen in the Newtonian cases at $\gamma_T = 1$, we find for power law rheologies that the symmetry between the upper and lower diapir hemispheres is maintained. However, the stress dependence of viscosity still modifies the shape of the diapir, from initially spherical to a prolate spheroid shape. During this transition, the diapir sinking velocity increases by about 50%, as shown by the red squares in Figure 1. This behavior was found for various power law exponents, n, ranging from 1 to 3.5.

[31] Figure 5 displays three snapshots of a typical evolution of the system for a power law viscous rheology with temperature-dependent viscosity and $\gamma_T = 10^3$. Although the viscous dissipation and temperature fields compare qualitatively well with the Newtonian case (Figure 3) three main differences can be noticed: (1) the maximum viscous

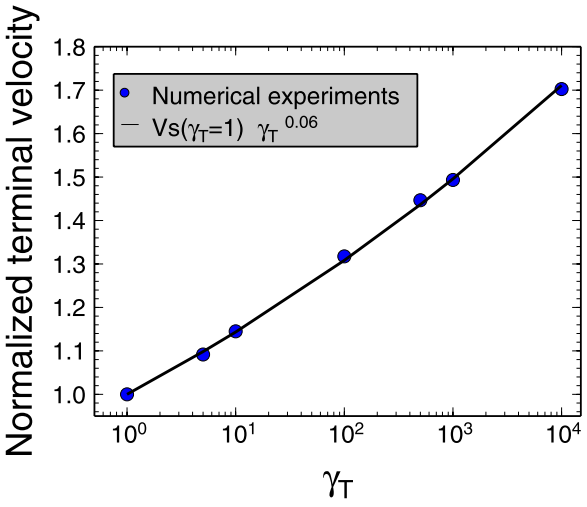

Figure 4. Normalized diapir terminal sinking velocities as a function of the sensitivity of temperature-dependent viscosity γ_T for Newtonian rheology. Symbols represent seven numerical experiments. The solid curve represents a power law fit (equation (10)).

dissipation and sinking velocities are greater by more than one order of magnitude than that of the Newtonian case (compare Figures 5a–5c and Figures 3a–3c); (2) the viscosity decrease due to the stress dependence extends up to several diapir radii (Figures 5g–5i); (3) because of the combination of stress- and temperature-dependent rheology, the shape of the diapir transitions from spherical to a prolate spheroidal cup (Figure 5).

2.3. Scaling Laws for Diapir Sinking Velocities

[32] We determine scaling laws for the diapir sinking velocity as a function of physical parameters. Similar to *Weinberg and Podlachikov* [1994, 1995], we express the diapir's terminal sinking velocity using a modified Stokes velocity for a frictionless fluid with an effective viscosity η_e:

$$V_s = \frac{\Delta\rho_c g r_d^2}{3\eta_e}\frac{f(\gamma_T)}{S}, \tag{11a}$$

$$\eta_e = \begin{cases} \eta_0 & \text{for } n = 1 \text{ or } (n > 1 \text{ and } \sigma_c < \sigma_T) \\ \eta_0\left(\frac{\sigma_c}{\sigma_T}\right)^{1-n} & \text{for } \sigma \geq \sigma_T \end{cases} \tag{11b}$$

$$S = [1.7(1 - n^{-2}) + n^{-1}]^n, \tag{11c}$$

where $\sigma_c = \Delta\rho_c g r_d/3$ is the characteristic stress imposed by the diapir and S is an empirical correction factor. The function f comes from equation (10).

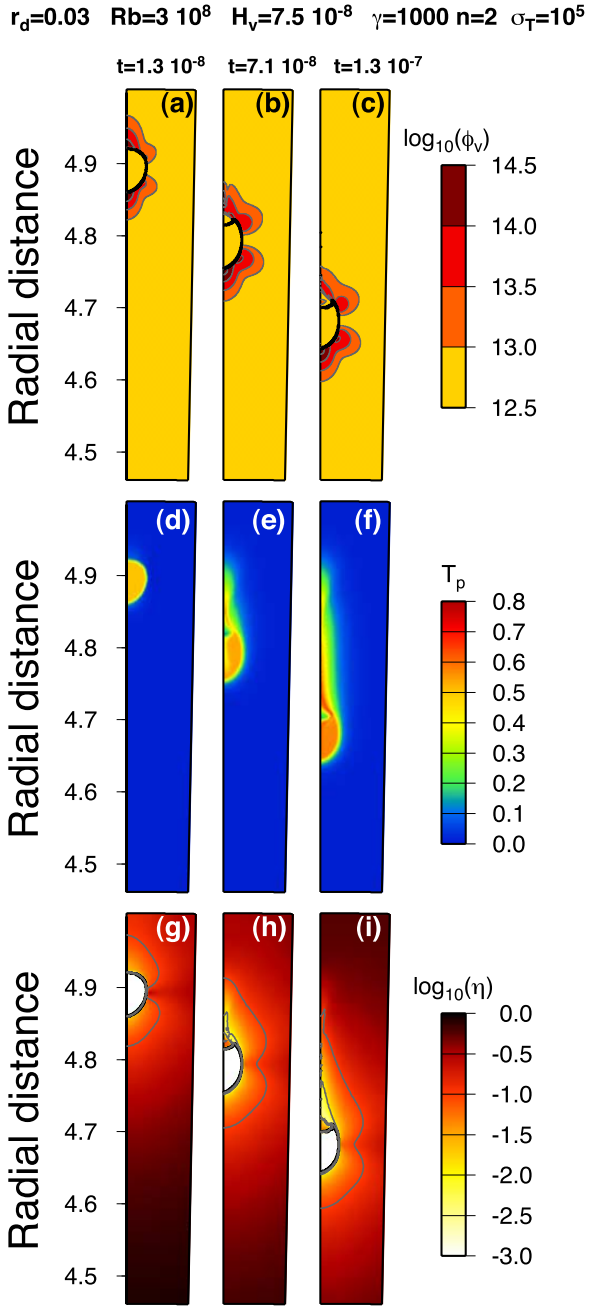

Figure 5. Results of the numerical experiment (close up view). The parameters are the same as in Figure 3 except for a power law rheology, with $n = 2$ and $\sigma_T = 10^5$. (a–c) Dimensionless viscous dissipation, (d–f) potential excess temperature, and (g–i) viscosity for three different dimensionless elapsed times (t = 1.3 × 10^{-8}, t = 7.1 × 10^{-8}, and t = 1.3 × 10^{-7}).

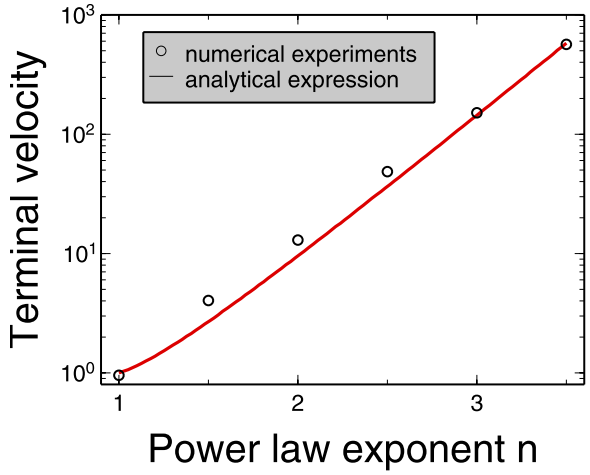

Figure 6. Normalized terminal sinking velocity as a function of the power law exponent n. Comparison between the numerical experiments (circles) and the analytical form of the diapir sinking velocity (solid curve, equation (11)).

[33] As shown in Figure 6, equations (11) describe well the results of our numerical experiments.

3. Melting and Metal-Silicate Equilibration

[34] Thermal models of terrestrial planet formation [*Coradini et al.*, 1983; *Sasaki and Nakazawa*, 1986; *Senshu et al.*, 2002] suggest that once the planet has reached a critical size of about 2000 km its radial thermal profile lies between its solidus and its liquidus. In this section we will therefore consider the case where metal diapirs sink through a silicate mantle whose temperature is above its solidus. In the following sections we develop a simplified semianalytical model to describe the dynamic behavior of the system as well as the consequences on metal-silicate equilibration during core formation.

3.1. Sinking Diapir Model

[35] On the basis of the results from the numerical experiments (section 2.2) we make the following assumptions in order to simplify the conservation equations: (1) adiabatic heating and density differences due to temperature are negligible, (2) viscosity variations due to the temperature or melt are confined to narrow zones and do not affect the flow significantly, and (3) the diapir shape always remains spherical and its viscosity is small compared to that of the surroundings.

[36] In addition, we now nondimensionalize the conservation equations using the following characteristic scales: V_s for velocity (equation (11)), r_d for distance, ρ_0 for density, and η_e/γ_T for viscosity (equation (11b)). An appropriate choice for the characteristic temperature scale is ΔT_e, the difference between the initial temperature of the diapir and T_r, the temperature at which silicates undergo a rheological transition where viscosity changes abruptly by several orders of magnitude. This transition corresponds to a critical melt fraction of about 60–70% [*Lejeune and Richet*, 1995; *Scott and Kohlstedt*, 2006].

[37] Using these new characteristic scales and under the assumptions listed above, the conservation of mass (equation (1)) remains unchanged but equations (2) and (3) simplify to:

$$\nabla p - \nabla \cdot \left(\eta \dot{\varepsilon}_{ij}\right) + C\vec{e_r} = 0, \tag{12}$$

and

$$\frac{DT}{DT} = \frac{1}{Pe_T}\nabla^2 T + \Pi_v \phi_v. \tag{13}$$

[38] The two dimensionless numbers which appear in equation (13) are a diapir thermal Péclet number:

$$Pe_T = \frac{V_s r_d}{\kappa_T}, \tag{14}$$

and the second number expresses the efficiency of viscous heating:

$$\Pi_v = \frac{V_s \eta_e}{\gamma_T r_d \Delta T_e \rho_0 C_p}. \tag{15}$$

[39] Equation (12) is now parameter free, indicating that once the sinking velocity is determined, the flow is known. Indeed, the solution of equations (1) and (12) subject to the assumptions made can be obtained analytically using a stream function formulation ψ [*Batchelor*, 1967] in spherical axisymmetric coordinates:

$$U = (U_r, U_\theta) = \frac{1}{r\sin\theta}\left(\frac{1}{r}\frac{\partial \psi}{\partial \theta}, -\frac{\partial \psi}{\partial r}\right),$$

where r is the dimensionless radius starting at the center of the diapir and θ is the angle measured from the diapir's upper pole.

[40] Following *Hadamard* [1911] and *Rybczynski* [1911] the flow inside and outside (past) the

spherical diapir is described by the two following dimensionless stream functions ψ_i and ψ_o:

$$\psi_i = -\frac{1}{4}\sin^2\theta r^2\left(r^2-1\right),$$

and

$$\psi_o = -\frac{1}{2}\sin^2\theta r(r-1).$$

[41] Using these analytical expressions is computationally inexpensive, and considering the flow past the spherical diapir also allows a great saving in computational time since the computational domain is greatly reduced and restricted only to the diapir plus a relatively small region around it.

[42] Equation (13) is solved by finite differences on a regular grid, in spherical axisymmetric geometry with the origin located at the center of the diapir. The computational domain is $r = [0.05, 3.5]$ and $\theta = [0, \pi]$. To avoid numerical instabilities, the small region between $r = 0$ and $r = 0.05$ is not modeled. However, this corresponds to a very small fraction of the diapir (~0.01%) and therefore does not affect our results significantly. We impose zero flux boundary conditions at all boundaries. The numerical implementation of equation (13) was successfully benchmarked for purely diffusive, purely advective or mixed cases, against steady and transient analytic solutions or against STAGYY.

3.2. Chemical Equilibration and Criteria for the Presence of Efficient Silicate Melt

[43] In order to investigate the chemical equilibration processes between the iron diapir and the surrounding silicate material, the above system of equations is supplemented by Fick's law, written here in nondimensional form:

$$\frac{D\chi}{Dt} = \frac{1}{Pe_\chi}\nabla^2\chi, \tag{16}$$

where χ is the concentration of a given chemical element (e.g., Ni, Co) and $Pe_\chi = V_s r_d/\kappa_c$ is the corresponding chemical Péclet number with κ_c being the chemical diffusivity of a given chemical element.

[44] As pointed out by *Rubie et al.* [2003], an essential condition for enabling chemical equilibration between a liquid metal diapir and the surrounding silicate material is the presence of silicate melt in sufficient volume proportion, $\phi_m \geq \phi_m^e$. The value of ϕ_m^e depends on various parameters, such as the geometry of the crystals and their distribution and orientation. For simplicity we consider that ϕ_m^e corresponds to the critical melt fraction at which the rheological transition in silicate occurs. In other words, ϕ_m^e is reached when $T = T_r$ (see section 3.1). When $\phi_m \geq \phi_m^e$, the equivalent diffusion coefficient of the mixture of melt and crystals is controlled by the diffusion coefficient of the melt phase [see *Crank*, 1986, and references therein]. On the contrary, if $\phi_m < \phi_m^e$, chemical diffusion processes are controlled by the very low chemical diffusivities in the solid silicate and chemical equilibration cannot be achieved in a reasonable time [*Karato and Murthy*, 1997] (i.e., within 10–100 Ma, the timescale of core formation for planets such as the Earth or Mars suggested by geochemical considerations [*Kleine et al.*, 2004a, 2004b]).

[45] As previously mentioned, we assume the initial temperature of the silicate surrounding the metal diapir lies between the silicate solidus and liquidus [*Coradini et al.*, 1983; *Sasaki and Nakazawa*, 1986; *Senshu et al.*, 2002], and below T_r, thus $\phi_m^e > \phi_m > 0$. Therefore metal silicate equilibration can only be achieved if temperature increases with time so that ϕ_m^e is reached. A quick inspection of equation (13) indicates that this requirement is met when viscous dissipation overcomes thermal diffusion, thus for $\Pi_v Pe_T > 1$.

3.3. Comparison With the Full Numerical Experiments

[46] To check if the three assumptions we make for the sinking diapir model are reasonable, we perform a comparison between the numerical experiments and the sinking diapir model for values of $\Pi_v Pe_T > 1$.

[47] Figure 7 displays four snapshots corresponding to four elapsed time or diapir sinking distance d_s for a numerical experiment with $\Pi_v = 0.7$, $Pe_T = 865$ and Newtonian rheology with $\gamma_T = 10^3$. In addition, we impose an abrupt viscosity decrease ($\eta = \eta_{min}$ for $T > T_r$) in order to mimic the rheological transition observed in silicates (see section 2.1). At $d_s = 0.6\ r_d$ (Figure 7a), silicate melt with $\phi_m \geq \phi_m^e$ (in red) is generated at the top of the diapir's upper hemisphere where viscous dissipation is maximum, as previously observed (see Figures 3a and 5a). As the diapir further sinks (Figure 7b), melt is also generated in the lower hemisphere and spreads around the diapir. The diapir leaves behind at melt tail. When $d_s = 5.2\ r_d$ (Figure 7c) the metal diapir is entirely surrounded by silicate melt and this configuration

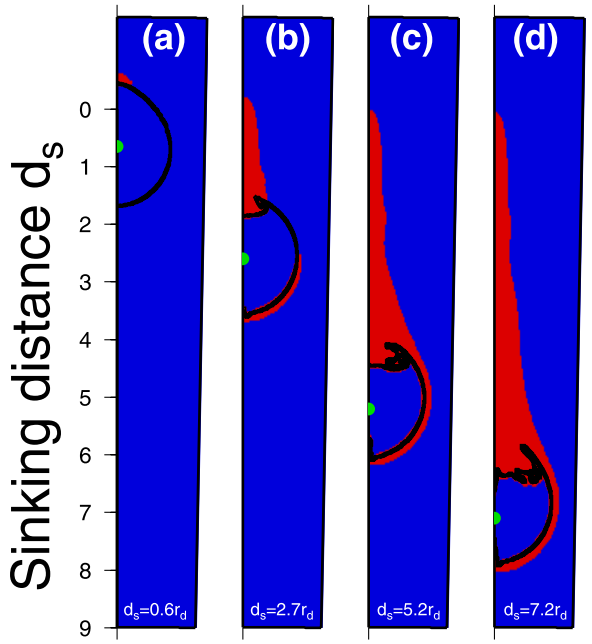

Figure 7. Results of the numerical experiment with $\Pi_v = 0.7$, $Pe_T = 865$, $n = 1$, and $\gamma_T = 10^3$. The snapshots correspond to four different sinking distances (d_s) of the metal diapir with the formation of silicate melt with $\phi_m \geq \phi_m{}^e$ (red). Black contours indicate the interface between the diapir and the surrounding silicate mantle. The green dots indicate the location of the diapir center of mass.

does not further evolve for greater sinking distances (Figure 7d). Note that having a rheological transition at $T = T_r$ always limits the maximum temperature to T_r in our experiments.

[48] Figure 8 displays the results of the semianalytical sinking diapir model with four snapshots corresponding to the same diapir sinking distances d_s and for the same parameters and rheology as in Figure 7. The generation and spreading of the silicate melt zone are in good agreement with the full numerical experiment. Moreover, similar to the numerical experiments, we find that the temperature quickly converges to T_r because of the abrupt viscosity decrease imposed at $T = T_r$.

[49] We performed additional comparisons between the full numerical experiments and the semianalytic sinking diapir model with values of $\Pi_v Pe_T$ ranging between 0 and 10^4. We find systematically that silicate melt is produced when $\Pi_v Pe_T > 1$ while no melt is produced when $\Pi_v Pe_T < 1$. This good agreement confirms that the assumptions made for the sinking diapir model are reasonable and provides a necessary condition for the presence of melting at $\Pi_v Pe_T > 1$.

3.4. Melt Geometry

[50] The requirement $\Pi_v Pe_T > 1$, is only a lower bound criteria for the presence of efficient melting. In fact, a more precise criteria can be formulated for the value of the parameter $\Pi_v Pe_T$ accounting for the melt geometry through the three following requirements:

[51] 1. The partial silicate melt (with $\phi^m \geq \phi^m{}_e$) should form a continuous layer, of thickness δ_m surrounding the metal diapir.

[52] 2. δ_m should not be greater than a fraction of the diapir's radius, say $\sim 0.1\ r_d$, in order for our scaling laws on V_s (equation (11)) to remain valid.

[53] 3. δ_m should be greater than the thickness of the chemical boundary layer located at the interface between the metal diapir and the silicate mantle so that chemical equilibration can proceed efficiently. This corresponds to a $\delta_m \sim \sqrt{\kappa_c r_d / V_s}$.

[54] Note that only the third criteria is a "hard" one. Indeed, if the melt layer is discontinuous, chemical equilibration can still proceed, however it will be delayed. In addition, having $\delta_m > 0.1 r_d$ also does not prevent chemical equilibration but our sinking diapir model is no longer valid since it falls outside the domain over which equation (11) is valid.

[55] Using the sinking diapir model we explored the parameter space of $\Pi_v = 0$–10^6 and $Pe_T = 10$–10^4. The results are summarized in Table 1 which shows that depending on the value of $Pe_T \Pi_v$, four categories can be distinguished

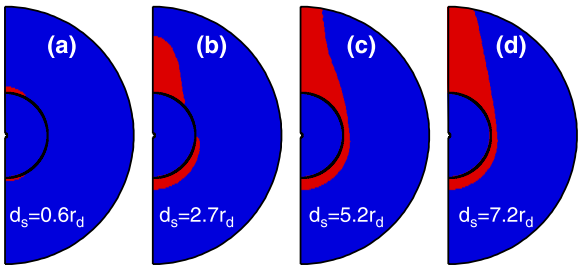

Figure 8. Results of the sinking diapir model with $\Pi_v = 0.7$, $Pe_T = 865$, $n = 1$, and $\gamma_T = 10^3$. The snapshots correspond to four different sinking distances (d_s) of the metal diapir with the formation of silicate melt with $\phi_m \geq \phi_m{}^e$ (red). Black contours indicate the interface between the diapir and the surrounding silicate mantle.

Table 1. Results From the Sinking Diapir Model: Silicate Melt Generation and Geometry Around the Metal Diapir[a]

$\Pi_v Pe_T$	Silicate Melt Geometry	Validity of Equation (11)
<1	no efficient melt generated	valid
∼1–10	disconnected melt pockets	valid
∼10–100	continuous thin melt layer	valid
>∼100	continuous thick melt layer	not valid

[a] This compilation was obtained for the parameter space $\Pi_v = 0 - 10^6$ and $Pe_T = 10 - 10^4$. Four categories are considered according the production of silicate melt and its geometry. The last category is the only one for which equation (11) is not applicable, because of the nonlocalization of low viscosity induced by the presence of the silicate melt. See text for further details.

according to the above melt criteria. Importantly, we find that the three geometrical melting criteria are met when

$$M = \Pi_v Pe_T \sim 10 - 100. \quad (17)$$

4. Metal-Silicate Equilibration During Core Formation

[56] In this section, we derive analytical expressions to determine the conditions under which a metal diapir can equilibrate with the surrounding silicate mantle during its descent. Following *Rubie et al.* [2003] we focus this analysis on the interdiffusion of the moderately siderophile element Ni, however it can be applied for any other chemical species for which the physical parameters are known.

4.1. Analytical Expression for Diapir Size, Equilibration Distances, and Equilibration Times

[57] We seek solutions of equations (13) and (16) that meet the three following criteria: (1) chemical equilibration (99%) between the diapir and the surrounding silicate material; (2) chemical equilibration time within $t_{eq}^{max} = z_{eq}^{max}/V_s < 100$ Ma, the upper bound for the timing of core formation for planets such as the Earth or Mars [*Kleine et al.*, 2004a, 2004b]; and (3) chemical equilibration distance with z_{eq}^{max} less than a few thousand kilometers.

[58] Combining equations (14), (15) and (17) yields general analytical solutions for the diapir's radius, r_{eq}, that satisfy the melting criteria and apply to both Newtonian ($n = 1$) and power law ($n > 1$) rheologies:

$$r_{eq} = \left[\frac{9S^2 M \eta_0 \kappa_T \Delta T_e \rho_0 C_p \gamma_T}{[\Delta\rho_c g f(\gamma_T \gamma_r)]^2} \left(\frac{\Delta\rho_c g}{3\sigma_T} \right)^{1-n} \right]^{\frac{1}{n+3}}, \quad (18)$$

where γ_r represents the abrupt viscosity decrease at the rheological transition. The total viscosity variation due to temperature/melt, $\gamma_r\gamma_T$, is accounted for in equation (18) through the function f (see equation (10)). Note that in equation (18) for power law rheology, n is replaced by 1 if $\sigma_c < \sigma_T$.

[59] To approximate the solution of equation (16) subject to the first criteria, we use the model developed by *Rubie et al.* [2003, equation 36], which yields an analytical expression for the equilibration time t_{eq} (i.e., the time necessary for a diapir of radius r_{eq} to equilibrate with the surrounding silicate mantle)

$$t_{eq} = \frac{1}{a} \ln\left(\frac{0.01 C_m^0 + b/a}{C_m^0 + b/a} \right), \quad (19)$$

where a and b are

$$a = \frac{V_s}{2r_{eq}} \left(\frac{F_m}{F_m + F_s/D_{ms}} - 1 \right)$$

$$b = \frac{V_s}{2r_{eq}} \frac{F_s C_s^0}{F_m + F_s/D_{ms}}$$

[60] $C_m^0 = 32700$ ppm and $C_s^0 = 42$ ppm are the initial Ni concentration in the metal diapir and in the silicate component, $D_{ms} = 28$ is the metal-silicate distribution coefficient. F_m and F_s are the mass fraction of the equilibrated metal and silicate components [*Rubie et al.*, 2003]:

$$F_m = \frac{(\rho + \Delta\rho_c) r_{eq}^3}{(\rho_0 + \delta\rho_c) r_{eq}^3 + 3 r_{eq}^2 \rho_0 \sqrt{2\kappa_c r_{eq}/V_s}}$$

$$F_s = 1 - F_m.$$

[61] For the derivation of the expressions for F_m, a and b the reader is referred to *Rubie et al.* [2003].

[62] Equation (19) was derived for centimeter-sized iron droplets sinking through a silicate magma ocean. However, it can be applied to a metal diapir of greater size sinking through a solid or partially

Table 2. Values of the Physical Parameters Used to Calculate the Results Shown in Figure 9[a]

Parameter	Value(s)/Range	Unit	Meaning
ρ_0	3500	kg m^{-3}	silicate density
$\Delta\rho_c$	4500	kg m^{-3}	compositional density contrast between metal and silicates
g	10	m s^{-2}	gravity acceleration
C_p	1000	J kg^{-1} K^{-1}	specific heat at constant pressure
κ_T	10^{-6}	m^2 s^{-1}	thermal diffusivity
κ_c	10^{-8}	m^2 s^{-1}	chemical diffusivity
η_0	10^7–10^{13}	Pa s	silicate viscosity at $T = T_0$
σ_T	10^4	MPa	transition strees
ΔT_e	25	K	$T_r - T_0$
n	1, 3.5	-	exponent for stress-dependent viscosity
γ_T	1	-	temperature sensitivity of the viscosity
γ_r	10^6	-	viscosity jump at the rheological transition
M	50	-	"efficient" melting criteria parameter

[a] T_0 is the initial temperature of the silicates surrounding the iron diapir. T_r is the temperature of the rheological transition at which viscosity decreases abruptly by a factor γ_r. See text for further details.

molten silicate mantle, as long as equation (17) is satisfied. This is indeed the case since equation (18) meets this requirement, by definition.

[63] Finally, using equations (19) and (11) we determine the equilibration distance

$$z_{eq} = V_s t_{eq}. \tag{20}$$

[64] Therefore, equations (18), (19) and (20) allow one to determine analytically the conditions under which Ni equilibration can be achieved during the sinking of an iron-rich diapir through a partially molten silicate mantle.

4.2. Implications for Core Formation

[65] The most uncertain physical parameter that influences the chemical equilibration processes between the sinking diapir and the silicate mantle is the viscosity of the silicate material, η_0. Indeed, this parameter can vary by several orders of magnitude depending on the temperature and melt fraction present [*Karato and Wu*, 1993; *Lejeune and Richet*, 1995; *Scott and Kohlstedt*, 2006]. Therefore, we have considered a plausible range of $\eta_0 = 10^{10\pm3}$ Pa s [*Karato and Murthy*, 1997] corresponding to a partially molten silicate mantle (i.e., for temperatures between the solidus and the critical melt fraction at which the rheological transition occurs).

[66] As previously mentioned, we focus on metal-silicate equilibration in a partially molten environment because this stage is likely to have occurred in terrestrial planets such as the Earth or Mars as suggested by accretional models [*Coradini et al.*, 1983; *Sasaki and Nakazawa*, 1986; *Senshu et al.*, 2002]

[67] The values for the remaining physical parameters used for the following calculation are listed in Table 2. To estimate ΔT_e we considered the temperature difference between the solidus and liquidus ΔT_e for peridotite, which ranges between ~100–200 K [*Zhang and Herzberg*, 1994] for a pressure range of 5–20 GPa. Assuming a linear increase of the melt fraction, ϕ_m, with increasing temperature $\Delta T_e = \phi_m^e \Delta T_{sl}$ can range between a few Kelvin to ~140 K. The chosen value within this range depends on the assumed temperature of the silicate mantle. Therefore we choose ΔT_e = 25 K, as listed in Table 2, which falls within this range. According to experimental work [*Lejeune and Richet*, 1995; *Scott and Kohlstedt*, 2006] and given the value of ΔT_e, the viscosity decrease due to the rheological transition is set to $\gamma_r = 10^6$ and γ_T is assumed to be close to unity (see Table 2).

[68] Figure 9a shows r_{eq} as a function of η_0 for Newtonian (solid line) and power law rheology with $\sigma_T = 10^4$ Pa and $n = 3.5$ (dashed line). r_{eq} ranges between 0.1 to almost 100 m depending on η_0 and the rheology considered. Note that the range of r_{eq} could be even broader, and could possibly reach kilometer sized values, depending on the choice of the physical parameters that enter into equation (18).

[69] The equilibration distance z_{eq} displayed in Figure 9b as a function of η_0 indicates that a ~1–100 m sized metal diapir would equilibrate

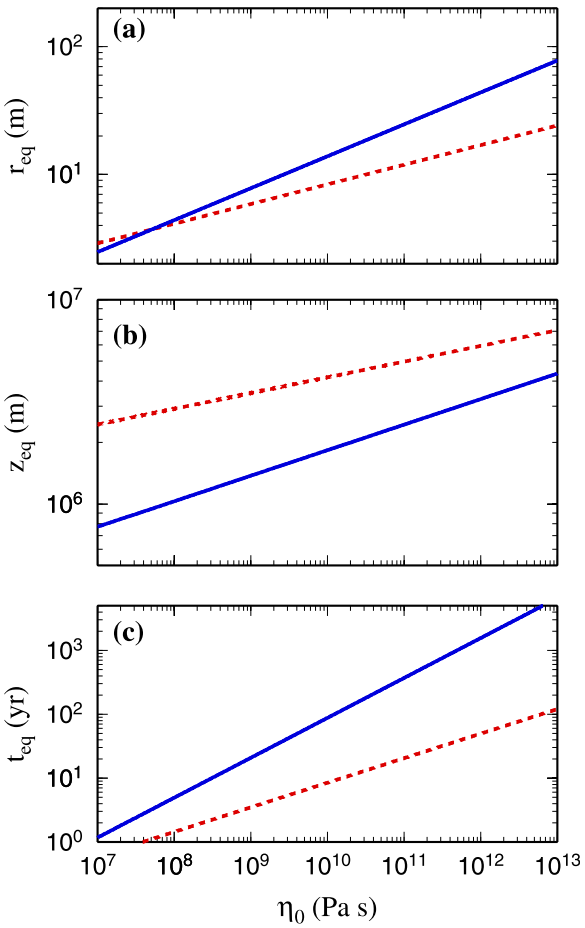

Figure 9. Conditions for metal-silicate equilibration during the sinking of the iron diapir for a plausible range of partially molten silicate mantle viscosities. Both Newtonian (solid lines) and power law rheologies (dashed lines) are considered. (a) Radius of the diapir obtained using equation (18), (b) equilibration distance (equation (20)), and (c) equilibration time (equation (19)) for a single diapir. We considered three criteria for chemical equilibration between the metal diapir and the surrounding silicates: (1) Chemical equilibration of Ni between the iron diapir and the surrounding silicates up to 99% (automatically satisfied by r_{eq}, see equation (18)). (2) Equilibration time t_{eq} less than 100 Ma, the timescale of core formation as suggested by *Kleine et al.* [2004a, 2004b]. (3) Equilibration distance z_{eq} less than a few thousand kilometers for a planet such as the Earth. See text and Table 2 for further details.

with the surrounding silicate mantle in a distance less than ~7000 km for both Newtonian and power law rheology, which satisfies our second criteria.

[70] Finally, Figure 9c indicates that the time necessary for these diapirs to equilibrate with the surrounding silicate mantle is less than 1000 years, well below t_{eq}^{max}.

[71] The analytical results displayed in Figures 9a–9c show that negative diapirism is a plausible scenario for core formation bounded by geochemical and mineral physics constraints for a diapir radius between 0.1 and 100 m. This range depends on the viscosity of the silicates surrounding the metal diapir which is poorly known.

[72] We considered uncertainties in other physical parameters with κ_c being 2–3 orders of magnitude smaller than the value listed in Table 2, ΔT_e = 10–120 K and for various values of σ_T = 10^4 Pa to 10^7 Pa and n = 1 – 3.5. We find that chemical equilibration remains possible for diapirs with a radius ranging from a meter to a kilometer in size.

[73] In addition to the partially molten scenario we have considered colder scenarios in which the silicate temperature T_0 is below its solidus, leading to much higher viscosities η_0 and higher ΔT_e. In this cases, equations (18) and (20) imply an increase of both r_{eq} and z_{eq}. As a consequence, it becomes difficult for the diapirs to fully equilibrate with the surrounding within reasonable distances (i.e., $z_{eq} < 10^7$ km). Note however that in these colder scenarios the diapirs can partially equilibrate with the surrounding silicates and therefore contribute to the metal silicate equilibration processes during core formation. The degree of partial equilibration between the iron diapir and the surrounding silicates can be determined using the model by *Rubie et al.* [2003].

[74] Note that we purposely did not consider additional complexities such as the depth/pressure dependence of physical parameters such as κ_c or ΔT_e because they are not well constrained under extreme P/T conditions. However, these influences can easily be incorporated in the analytical expressions derived in this study since equations (18) and (19) should remain valid for a smooth change in physical parameters with depth/pressure (e.g., η_0, γ_T, κ_c).

[75] So far, we focused on the ability of a single metal diapir to equilibrate with the surrounding which is a necessary condition for a global metal-silicate equilibration during core formation by negative diapirism.

[76] In order to extend these results for multiple diapirs, we have estimated β, the volume fraction of silicates that would equilibrate with sinking iron diapirs, following *Karato and Murthy* [1997]. Assuming by simplicity that all the iron diapirs

have the same size, r_{eq} and a final metallic core radius r_{core} = 3500 km, $\beta \sim r_{core}\sqrt{\kappa_c r_{eq}^{-3} V_s^{-1}}$ as in the work by *Karato and Murthy* [1997]. Using this expression, the parameter values listed in Table 2 and the values for r_{eq} displayed in Figure 9 we find that β is always greater than 100% (i.e., complete global metal silicate equilibration is achieved), thus indicating that our results for a single diapir would translate for multiple diapirs of identical size.

[77] Obviously, core formation by negative diapirism implies the sinking of a large number of diapirs of various sizes and therefore with their own ability to equilibrate. Additional complexities might also occur with the possibility of multiple interactions between the nearby diapirs, including merging. All these effects are not included in the simple calculation above. Nevertheless, the scaling laws we derived can be used in the case of multiple diapirs which may interact and merge during their sinking [e.g., *Senshu et al.*, 2002].

5. Conclusions

[78] We have investigated the dynamics of core formation by negative diapirism using high-resolution numerical modeling and analytical theory. Our results show that the conversion of potential to thermal energy via viscous heating generates a temperature increase at the interface between the diapir and the silicate mantle. This localized temperature increase can generate sufficient silicate melt fraction and locally increases the silicate chemical diffusivity. As a result, chemical equilibration is enhanced during the sinking of the metal diapir in a solid or partially molten silicate mantle.

[79] We derived general scaling laws for the diapir terminal sinking velocity which describe well the results of our numerical experiments for various Newtonian and power law rheologies (equation (11)). We subsequently used these scaling laws to derive a simple semianalytical sinking diapir model which reproduces well the results of our numerical experiments. This diapir sinking model has provided an analytical expression for the radius of a metal diapir that favors equilibration with the surrounding silicate mantle (equation (18)).

[80] Using these analytical expressions together with the equilibration model developed by *Rubie et al.* [2003] (equation (19)), as well as our scaling law for the diapir sinking velocity, we have shown that negative diapirism is a plausible scenario for core formation. All these analytical expressions can easily be incorporated into accretional models to monitor the chemical evolution of a growing terrestrial planet during the stages of core formation.

[81] We show that for a range of silicate viscosities $\eta_0 = 10^{10\pm3}$ Pa s corresponding to a partially molten silicate mantle, core formation with metal silicate equilibration can be achieved within the timescales suggested by geochemical constraints (i.e., less than 100 Ma). Therefore negative diapirism can contribute significantly to metal-silicate equilibration processes during core formation.

Acknowledgments

[82] The authors are grateful to the associate editor and to an anonymous referee whose comments improved the clarity of our manuscript. Henri Samuel was supported by the funds from the PLANETZ INIT program. Figures were made with the Generic Mapping Tools [*Wessel and Smith*, 1995].

References

Batchelor, G. K. (1967), *An Introduction to Fluid Dynamics*, 615 pp., Cambridge Univ. Press, Cambridge, U. K.

Canup, R. (2004), Simulations of a late lunar-forming impact, *Icarus*, *168*, 433–456.

Chang, I. (1961), On the wall effect correction of the stokes drag formula for axially symmetric bodies moving inside a cylindrical tube, *Z. Angewandte Math. Phys.*, *12*, 6–14.

Coradini, A., F. Costanzo, and P. Lanciano (1983), Earth and Mars: Early thermal profiles, *Phys. Earth. Planet. Inter.*, *31*, 145–160.

Crank, J. (1986), *The Mathematics of Diffusion*, 2nd ed., Oxford Univ. Press, Oxford, U. K.

Daly, S. F., and A. Raefsky (1985), On the penetration of a hot diapir through a strongly temperature-dependent viscosity medium, *Geophys. J. R. Astron. Soc.*, *83*, 657–681.

Gerya, T. V., and D. A. Yuen (2003), Characteristics-based marker-in-cell method with conservative finite-differences schemes for modeling geological flows with strongly variable transport properties, *Phys. Earth. Planet. Inter.*, *140*, 293–318.

Golabek, G. J., H. Schmeling, and P. J. Tackley (2008), Earth's core formation aided by flow channelling instabilities induced by iron diapirs, *Earth Planet. Sci. Lett.*, in press.

Hadamard, J. (1911), Mouvement permanent lent d'une sphère liquide et visqueuse dans un liquide visqueux, *C. R. Acad. Sci.*, *152*, 1735–1738.

Halliday, A. N. (2004), Mixing, volatile loss and compositional change during impact-driven accretion of the Earth, *Nature*, *427*, 505–509.

Hoïnk, T., J. Schmalzl, and U. Hansen (2006), Dynamics of metal-silicate separation in a terrestrial magma ocean, *Geochem. Geophys. Geosyst.*, *7*, Q09008, doi:10.1029/2006GC001268.

Honda, R., H. Mizutani, and T. Yamamoto (1993), Numerical simulation of Earth's core formation, *J. Geophys. Res.*, *98*, 2075–2089.

Karato, S.-I., and R. V. Murthy (1997), Core formation and chemical equilibrium in the Earth—I. Physical considerations, *Phys. Earth. Planet. Inter.*, *100*, 61–79.

Karato, S.-I., and P. Wu (1993), Rheology of the upper mantle: A synthesis, *Science*, *260*, 771–778.

Kleine, T., K. Mezger, C. Münker, H. Palme, and A. Bischoff (2004a), ^{182}Hf-^{182}W isotope systematics of chondrites, eucrites, and martian meteorites: Chronology of core formation and early mantle differentiation in Vesta and Mars, *Geochim. Cosmochim. Acta*, *68*, 2935–2946.

Kleine, T., K. Mezger, H. Palme, and C. Münker (2004b), The W isotope evolution of the bulk silicate Earth: Constraints on the timing and mechanisms of core formation and accretion, *Earth Planet. Sci. Lett.*, *228*, 109–123.

Lejeune, A.-M., and P. Richet (1995), Rheology of crystal-bearing silicate melts: An experimental study at high viscosities, *J. Geophys. Res.*, *100*, 4215–4229.

Mahon, K. I., T. M. Harrison, and A. D. Drew (1988), Ascent of a granitoid in a temperature varying medium, *J. Geophys. Res.*, *93*, 1174–1188.

Morris, S. (1982), The effects of a strongly temperature-dependent viscosity on a slow flow past a sphere, *J. Fluid Mech.*, *124*, 1–26.

Ribe, N. M. (1983), Diapirism in the Earth's mantle: Experiments on the motion of a hot sphere in a fluid with temperature-dependent viscosity, *J. Volcanol. Geotherm. Res.*, *16*, 221–245.

Ricard, Y., O. Sramek, and F. Dubuffet (2008), Multiphase model of planetary evolution, *Geophys. Res. Abstr.*, *10*, EGU2008-A-06,194.

Ringwood, A. E. (1966), Chemical evolution of terrestrial planets, *Geochim. Cosmochim. Acta*, *30*, 41–104.

Rubie, D. C., H. J. Melosh, J. E. Reid, C. Liebske, and K. Righter (2003), Mechanisms of metal-silicate equilibration in the terrestrial magma ocean, *Earth Planet. Sci. Lett.*, *205*, 239–255.

Rubie, D. C., F. Nimmo, H. J. Melosh (2007), Formation or Earth's core, in *Treatise on Geophysics*, vol. 9, edited by G. Schubert and D. J. Stevenson pp. 51–90, Elsevier, New York.

Rybczynski, W. (1911), Über die fortschreitende bewegung einer flüssigen Kugel in einen Medium, *Bull. Acad. Sci. Cracovie*, *1*, 40–46.

Sasaki, S., and K. Nakazawa (1986), Metal-silicate fractionation in the growing Earth: Energy source for the terrestrial magma ocean, *J. Geophys. Res.*, *91*, 9231–9238.

Scott, T., and D. L. Kohlstedt (2006), The effect of large melt fraction on the deformation behavior of peridotite, *Earth Planet. Sci. Lett.*, *246*, 177–187.

Senshu, H., K. Kuramoto, and T. Matsui (2002), Thermal evolution of a growing Mars, *J. Geophys. Res.*, *107*(E12), 5118, doi:10.1029/2001JE001819.

Solomatov, V. S. (2000), Fluid dynamics of a terrestrial magma ocean, in *Origin of the Earth and Moon*, edited by R. Canup and K. Righter, pp. 323–338, Univ. of Ariz. Press, Tucson.

Stevenson, D. J. (1981), Models of the Earth's core, *Science*, *214*, 611–619.

Tackley, P. J., and S. D. King (2003), Testing the tracer ratio method for modeling active compositional fields in mantle convection simulations, *Geochem. Geophys. Geosyst.*, *4*(4), 8302, doi:10.1029/2001GC000214.

Weinberg, R. F., and Y. Y. Podlachikov (1994), Diapiric ascent of magmas through power law crust and mantle, *J. Geophys. Res.*, *99*, 9543–9559.

Weinberg, R. F., and Y. Y. Podlachikov (1995), The rise of solid state diapirs, *J. Struct. Geol.*, *17*, 1183–1195.

Wessel, P., and W. H. F. Smith (1995), New version of the generic mapping tools released, *Eos Trans. AGU*, *76*(33), 329.

Wood, B. J., M. Walter, and J. Wade (2006), Accretion of the Earth and segregation of its core, *Nature*, *441*, 825–833.

Zhang, J., and C. Herzberg (1994), Melting experiments on anhydrous peridotite KLB-1 from 5.0 to 22.5 GPa, *J. Geophys. Res.*, *99*, 17,729–17,742.

Ziethe, R., and T. Spohn (2007), Two-dimensional stokes flow around a heated cylinder: A possible application for diapirs in the mantle, *J. Geophys. Res.*, *112*, B09403, doi:10.1029/2006JB004789.